JOURNAL OF GEOPHYSICAL RESEARCH, VOL. 92, NO. B9, PAGES 8903-8911, AUGUST 10, 1987

TILL BENEATH ICE STREAM B
1. PROPERTIES DERIVED FROM SEISMIC TRAVEL TIMES

D. D. Blankenship, C. R. Bentley, S. T. Rooney, and R. B. Alley

Geophysical and Polar Research Center, University of Wisconsin-Madison

Abstract. Seismic experiments conducted on ice stream B, part of the marine ice sheet of West Antarctica, show a meters-thick layer immediately beneath the 1000-m-thick ice. A seismic experiment consisting of wide-angle reflection profiling along a line parallel to ice stream flow was conducted to determine the properties of this layer. Inversion of seismic travel times yields a compressional wave speed of less than 1700 m s^{-1} and a shear wave speed less than 160 m s^{-1} for the layer. These very low wave speeds imply that the material in the layer is highly porous and is saturated with water at a high pore pressure. Based on wave speeds in other saturated, unconsolidated sediments, we believe that a porosity substantially greater than 0.32, probably around 0.4, and an excess of overburden pressure over pore pressure of only 50 kPa (0.5 bar) characterize the layer at this location.

1. Introduction

A thorough understanding of the marine ice sheet of West Antarctica is essential for global climatology as well as for glaciology. The goal of a research project carried out since 1983 by the University of Wisconsin (UW) in conjunction with The Ohio State University, NASA, and the University of Chicago is to study the portion of the West Antarctic ice sheet that lies along the Siple and Gould coasts and extends from the Rockefeller Plateau down to the Ross Ice Shelf (Figure 1). This region is dominated by the "Ross" ice streams [Bentley, this issue], which represent portions of the inland ice sheet that flow much more rapidly than the surrounding ice. Because these ice streams play a pivotal role in the dynamics of this whole section of Antarctica, an understanding of the processes that form, maintain, and destroy them is essential for a thorough understanding of the West Antarctic ice sheet. It is also likely that such ice streams have played an important part in the development and disappearance of ice sheets in the past.

The field work associated with this cooperative project has so far concentrated on ice stream B. More specifically, the UW Geophysical and Polar Research Center has been conducting extensive geophysical investigations at the Upstream B (UpB) camp on ice stream B (Figure 1). Both active and passive seismology have been important elements of these investigations. Here we present in detail the results of one of the active seismic experiments performed during the 1983-1984 field season. Preliminary versions of some of these results are reported by Blankenship et al. [1986], where the discovery of a thin layer of unconsolidated, water-saturated sediment at the base of the ice stream is outlined. Rooney et al. [this issue] show, based on active seismic experiments performed during the 1984-1985 field season, that this layer is essentially continuous beneath the ice stream in a direction transverse to ice flow. Alley et al. [1986, this issue (a)] conclude that this layer is a subglacial till that is both deforming and eroding its bed. Alley et al. [1986, this issue (b)] argue that this till plays a dominant role in the dynamics of ice stream B.

Paper number 6B6179.
0148-0227/87/006B-6179$05.00

2. Field Work

During the 1983-1984 field season at UpB, seismic experiments were performed along the lines shown in Figure 2. One of these experiments consisted of "wide-angle" reflection profiling along a line that was parallel to the flow of the ice stream (line SA on Figure 2). The primary goal of this experiment was to determine the geometry and seismic properties of a layer at the base of the ice stream that was discovered during seismic surveys earlier in the season [Blankenship et al., 1986, Figure 2]. Blankenship et al. [1986] and Alley et al. [1986] give reasons to believe that the layer is composed of till, and we will refer to it as till hereafter.

For this experiment we used a receiving spread that was 690 m in length with geophones spaced every 30 m. Sources were small (0.45 kg) explosive charges detonated in boreholes that were 15-18 m deep. The source and the receiving spread were moved symmetrically away from the center of the line (the intersection of SA, SB, and SC in Figure 2) in 360-m increments. The maximum source-receiver offset was 3960 m, so the maximum angle of incidence in the 1-km-thick ice was about 60°. This shooting geometry produced six rays reflecting from each of 24 points along the bottom of the ice stream. These reflection points were located approximately 15 m apart along a region of the bottom that extended 360 m upstream from the center of our line.

To optimize the recording of both compressional waves (P waves) and shear waves (S waves), the entire experiment was repeated for each of three different geophone orientations: vertical, horizontal longitudinal, and horizontal transverse. For all three orientations one 28-Hz geophone per takeout was used; these geophones were damped to 60% of critical and responded linearly to frequencies up to 420 Hz. All recording was done using a digital seismic recorder developed at the Geophysical and Polar Research Center. Each of the 24 channels of the receiving spread was re-

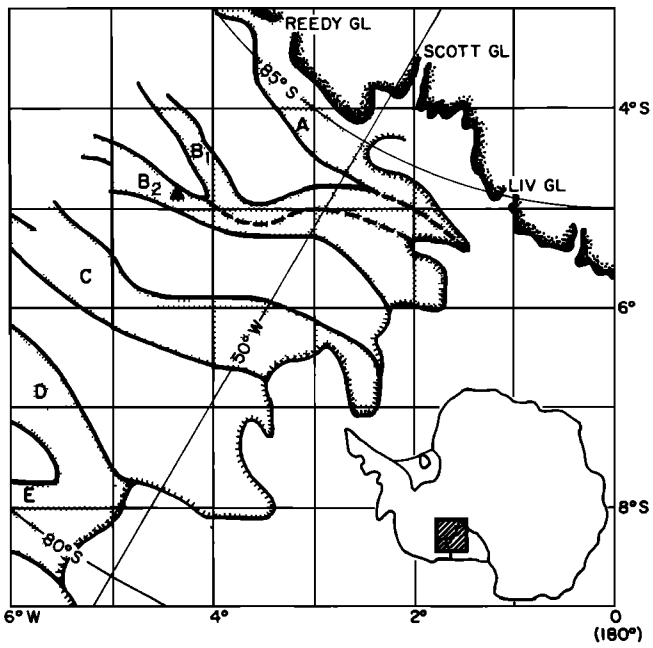

Fig. 1. The Siple Coast of West Antarctica. The "Ross" ice streams are lettered A, B, C, D, and E. The triangle denotes the location of the Upstream B camp. Simplified from Shabtaie and Bentley [1986].

corded at 2500 samples per second. Timing information broadcast from the shooting station also was recorded digitally.

3. Data Analysis

3.1. Description of Seismograms

Some of the seismograms recorded during the "wide-angle" experiment are presented in essentially "raw" form in Figures 3 and 4; the only postprocessing has been the application of a band-pass filter.

The seismograms in Figure 3 clearly show a P wave reflecting from the bottom of the ice (denoted $\grave{P}\acute{P}$) followed about 10 ms later by another reflection (denoted $\grave{P}\grave{P}\acute{P}\acute{P}$) from the bottom of the till. Two "ghost" arrivals, also separated by about 10 ms, follow $\grave{P}\acute{P}$ and $\grave{P}\grave{P}\acute{P}\acute{P}$; a ghost is an arrival that has been reflected first from the surface above the shot. (Following earthquake notation, we will denote P wave reflection from the surface above the shot by a lower case p; s has the analogous meaning for an S wave. Thus the ghost of $\grave{P}\acute{P}$ is $p\grave{P}\acute{P}$, etc.)

The time delay for $p\grave{P}\acute{P}$ depends on the P wave velocity v_p in the firn above the shot. Table 1 presents both $v_p(z)$ and $v_s(z)$ for the firn at UpB as determined by seismic refraction experiments, where z is depth below the ice-air surface (S. Anandakrishnan, personal communication, 1986). Because the velocities above 20 m are much lower than in the deeper firn, the ray path above the shot is very nearly vertical; thus the delay time for $p\grave{P}\acute{P}$ can be estimated closely by twice the "uphole" time (the time to travel from the source to the surface). The uphole time for our shots calculated from Table 1 and the measured borehole depth is approximately 10 ms; $p\grave{P}\acute{P}$ and $p\grave{P}\grave{P}\acute{P}\acute{P}$ arrive about 20 ms after $\grave{P}\acute{P}$ and $\grave{P}\grave{P}\acute{P}\acute{P}$ (Figure 3).

The seismograms in Figure 4 show some of the S wave arrivals recorded during the "wide-angle" experiment. The first arrival is $\grave{S}\acute{S}$, the S wave reflected from the bottom of the ice. The second arrival is not, however, the S wave reflected from the bottom of the subglacial till ($\grave{S}\grave{S}\acute{S}\acute{S}$), but rather $s\grave{S}\acute{S}$. The third and fourth arrivals, coming about 100 ms after the first pair, are $\grave{S}\grave{S}\acute{S}\acute{S}$ and $s\grave{S}\grave{S}\acute{S}\acute{S}$, respectively. An expected uphole time for S waves of 18 ms has been calculated from $v_s(z)$ given in Table 1 and the borehole depth. The ghosts in Figure 4 can be seen to arrive 40-45 ms after both $\grave{S}\acute{S}$ and $\grave{S}\grave{S}\acute{S}\acute{S}$, which is close to, but slightly more than, twice the estimated uphole time. The discrepancy can easily be explained by the uncertainty in the determination of the S wave velocity for the firn at depths of less than 2 m presented in Table 1 (S. Anandakrishnan, personal communication, 1986).

Two interesting observations can be made directly from an examination of the seismograms in Figures 3 and 4. These are (1) that the near-vertical travel time for S waves in the till is approximately 10 times greater than for P waves; i.e., $v_p/v_s \simeq 10$, and (2) that the travel time through the layer for both P and S waves (~10 ms

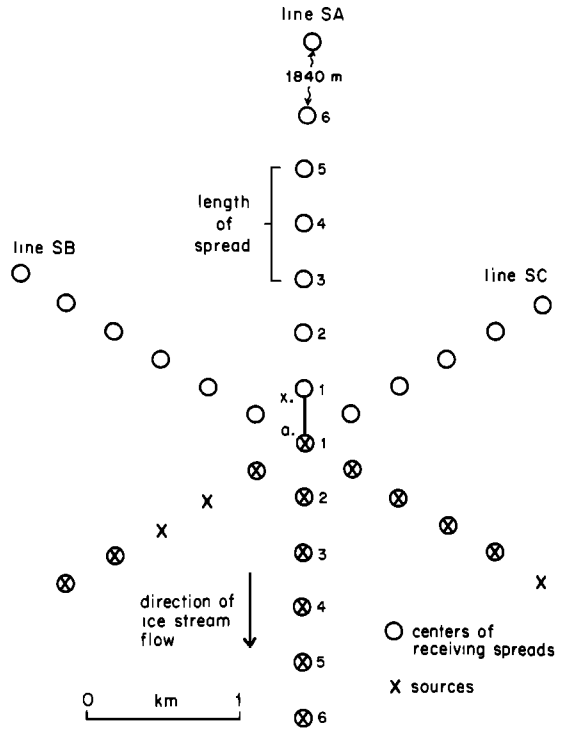

Fig. 2. Source and receiving spread locations for the active seismic experiments performed at Upstream B during the 1983-1984 field season. The "wide-angle" reflection work described here was undertaken along line SA. The numbers indicate the source and the center of the corresponding receiving spread as they were moved symmetrically away from the intersection of lines SA, SB, and SC. The 24 reflection points (lettered a to x) fall along the solid line parallel to flow.

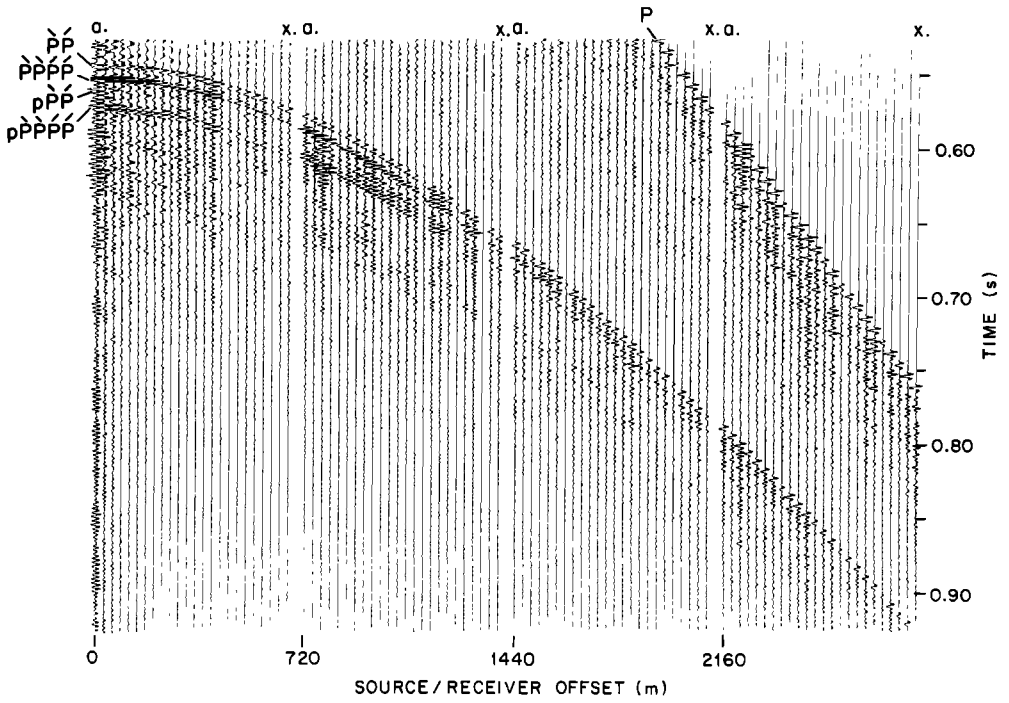

Fig. 3. Seismograms depicting "wide-angle" reflections of P waves. PP is the reflection from the base of the ice, and PPPP is the reflection from the base of the till; pPP and pPPPP are the respective ghosts for these arrivals. The traces corresponding to reflection points a and x of Figure 2 are labeled for each seismogram. P is the direct wave traveling through the ice.

and ~100 ms, respectively) changes little, if at all, with angle of incidence; this implies that both v_p and v_s in the till are much smaller than v_p and v_s in the ice.

3.2. Inversion Procedure

For inversion of the travel times to obtain the wave velocities in the till and the thickness of the layer, a combination of standard two-dimensional ray tracing, the multidimensional form of Newton's method, and generalized inverse techniques was used.

The forward problem of calculating the travel times of seismic rays along a path of specified type (e.g., PP) through the firn-ice-till system was solved by defining, at each of a sequence of boundary depths $z = b_i$, a boundary slope a_i relative to the surface and $(v_p)_i$ (or $(v_s)_i$) and its vertical gradient. For each combination of source and receiver positions a ray was initially traced (following the techniques of Clay and Medwin [1977]) along the Snell's law path from the source using the horizontal slowness observed at the receiver as the initial value of the ray parameter. The ray parameter at the source was then adjusted until the ray emerged at the receiver.

Once the forward problem was solved, it was linearized using a multidimensional form of Newton's method [Dahlquist and Björck, 1974]. A model was then constructed by specifying a ray path (e.g., PP) and flagging certain of the parameters used to describe the firn-ice-till system as model parameters (the kth parameter is denoted p_k). To apply Newton's method to this

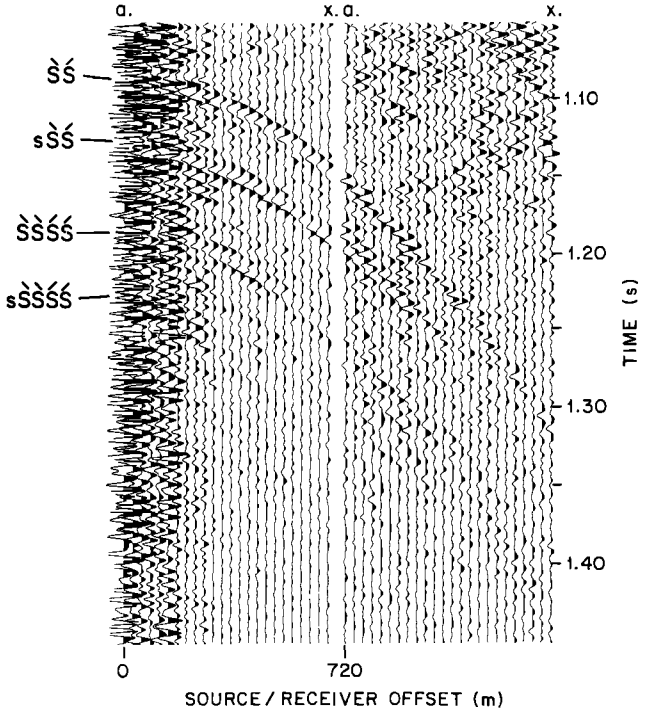

Fig. 4. Seismograms depicting "wide-angle" reflections of S waves. SS is the reflection from the base of the ice, and SSSS is the reflection from the base of the till; sSS and sSSSS are the respective ghosts for these arrivals. The traces corresponding to reflection points a and x of Figure 2 are labeled for each seismogram.

TABLE 1. Wave velocities $v_p(z)$ and $v_s(z)$ for the Firn on Ice Stream B

z, m	v_p, m/s	z, m	v_s, m/s
0.0	854	0.0	542
2.1	1076	2.0	668
4.8	1451	5.2	919
7.8	1845	6.9	1034
10.8	2216	10.1	1224
16.0	2790	13.0	1365
20.0	3131	15.5	1468
25.2	3424	19.8	1605
30.0	3590	25.3	1727
35.0	3703	29.8	1798
40.0	3777	35.1	1855
45.0	3826	40.0	1886
60.0	3861	45.1	1898

model, the partial derivatives of the travel time t (for a particular path) with respect to the model parameters, $\partial t/\partial p_k$, have to be calculated. These derivatives are obtained numerically using the difference equation

$$\frac{\partial t}{p_k} = \frac{t(p_k + \epsilon_k) - t(p_k - \epsilon_k)}{2\epsilon_k} \quad (1)$$

where ϵ_k is a perturbation for p_k. If ϵ_k is not carefully determined, equation (1) will be numerically unstable. For ϵ_k we used perturbations in the parameters which, for an approximation of the firn-ice-till system, corresponded to about 1% of the estimated error in our travel time observations; this physically based technique has proven to be quite stable. The form of Newton's approximation we used can be stated as

$$\sum_{k=1}^{n} \frac{\partial t_j}{\partial p_k} \delta p_k = \Delta t_j \quad (2)$$

where j is the index of a particular travel time observation, Δt_j is the residual of t_j compared to the value for the forward problem, δp_k is a variation in p_k, and n is the number of model parameters.

For m travel time observations, equation (2) is a system that can be represented by

$$\vec{G}\,\vec{p} = \vec{d} \quad (3)$$

where the elements of the kernel $\vec{G}$ are the partial derivatives, the elements of $\vec{p}$ are the δp_k, and the elements of $\vec{d}$ are the Δt_j. Solutions were obtained by first making initial guesses of the p_k and then using equation (1) and ray tracing to calculate $\vec{G}$ and $\vec{d}$. Equation (3) was then solved for $\vec{p}$ using generalized inverse techniques. (For computational stability we utilized the Moore-Penrose pseudoinverse of $\vec{G}$ constructed from its singular value decomposition [Forsythe et al., 1977]; singular values less than m times the machine precision were considered negligible.) The elements of $\vec{p}$ were then used to correct the model parameters, and the process was repeated until the sample variance of the travel time residuals,

$$s^2 = \frac{\sum_{j=1}^{m} |t_j|^2}{m - n} \quad (4)$$

was minimized. Repetition was halted when the value of s^2 increased for successive iterations. The method described above usually "converges," at least to a local minimum of s^2. If the initial guesses for the model parameters are "sufficiently close" to the true values, the final model parameters correspond to an absolute minimum of s^2. For our simple reflection paths through the firn-ice-till system the range of sufficiently close initial guesses was quite large.

Generalized inverse theory was used instead of standard multiple-regression techniques based on the normal equation because of a concern that some of the model parameters might be interdependent. The model resolution matrix and the unit-covariance matrix [Aki and Richards, 1980] were used to describe, respectively, the interdependencies and the error in the model parameters. These matrices are a straightforward by-product of the singular value decomposition of $\vec{G}$ [Menke, 1984].

3.3. Travel Time Inversion

The signal-to-noise ratio of the seismograms was good enough to allow both P and S wave arrivals from each of the 24 reflection points to be picked. $\grave{P}\acute{P}$ and $\grave{P}\grave{P}\acute{P}\acute{P}$ were identified at distances up to 2850 m (Figure 3); $\grave{S}\acute{S}$ and $\grave{S}\grave{S}\acute{S}\acute{S}$ were identifiable up to 1410 m (Figure 4). The travel times were obtained by picking the first trough of $\grave{P}\acute{P}$ and $\grave{S}\acute{S}$ and the first peak of $\grave{P}\grave{P}\acute{P}\acute{P}$ and $\grave{S}\grave{S}\acute{S}\acute{S}$. This was done because a phase reversal should occur between these arrivals, since the acoustic impedance in the till is less than in the ice and presumably less also than in the substrate. Analysis done by one of us (S.T.R.) of the autocorrelation functions of many observations of $\grave{P}\acute{P}$ and $\grave{P}\grave{P}\acute{P}\acute{P}$ tends to substantiate this for compressional waves. We estimate the error in picking P waves to be approximately one half of a sample interval ($\pm$0.2 ms) and the error in picking S waves to be two or three sample intervals ($\pm$1 ms). Each pick was corrected to a zero crossing by subtracting 2.4 ms for P waves and 7.7 ms for S waves; these values were determined from an analysis of the respective source wavelets.

The inversion procedures described in the previous section were first applied to about 90 observations of $t(\grave{P}\acute{P})$. The model parameters for this inversion were the slope (a_{ice}) and depth (b_{ice}) of the bottom of the ice stream and $(v_p)_{ice}$ in the ice; $v_p(z)$ in the firn (Table 1) was not varied. Newton's method applied to our observations of $t(\grave{P}\acute{P})$ easily converged, resulting in a unique solution for each of the three model parameters. The values were

$$a_{ice} = -0.001 \pm 0.001$$

$$b_{ice} = 1033.7 \pm 0.2 \text{ m}$$

$$(v_p)_{ice} = 3831.4 \pm 0.6 \text{ m s}^{-1}$$

TABLE 2. F for Models With Fixed $(v_p)_{till}$

$(v_p)_{till}$, m/s	s_2^2, ms^2	$F = s_2^2/s_1^2$
3500	1.57	10.6
3000	0.78	5.3
2500	0.41	2.8
2000	0.24	1.6
1800	0.21	1.4
1600	0.18	1.2
1400	0.16	1.1
1200	0.15	1.0

The quantity s_2^2 is the sample variance for the models with fixed $(v_p)_{till}$; s_2^2 (0.15 ms^2) is the sample variance for the "best fit" model.

with

$$s^2(\hat{P}\hat{P}) = 9.4 \times 10^{-8}\ s^2$$

The standard deviation, 0.3 ms, is roughly our estimated picking precision. The standard deviations for the model parameters were obtained by mapping $s^2(\hat{P}\hat{P})$ into variances for the model parameters using the unit-covariance matrix.

Using the parameters for the ice determined from $t(\hat{P}\hat{P})$, the 90 or so observations of $t(\hat{P}\hat{P}\hat{P}\hat{P})$ were inverted. The model parameters for this inversion were the basal slope and thickness of the till (a_{till} and h_{till}, respectively) and $(v_p)_{till}$. Newton's method again converged; however, the resulting solution vector was nonunique. Whereas the determination of a_{till} was unique, h_{till} and $(v_p)_{till}$ were interdependent. The values were

$$a_{till} = -0.002 \pm 0.001$$

$$h_{till} = 4.6\ \text{m} + (0.005\ \text{s})[(v_p)_{till} - 949\ \text{m s}^{-1}] \quad (5)$$

with

$$s^2(\hat{P}\hat{P}\hat{P}\hat{P}) = 1.5 \times 10^{-7}\ s^2$$

giving a standard deviation, 0.4 ms, that again is consistent with our estimated picking precision. The error for a_{till} contains contributions not only from the unit-covariance matrix for this inversion but also from the variance of a_{ice}. An error estimate for h_{till} is not possible without knowing $(v_p)_{till}$.

Physically, equation (5) implies that $(v_p)_{till}$ is so much less than $(v_p)_{ice}$ that even rays incident on the base of the ice at large angles travel essentially vertically through the till. We can only determine an upper bound to $(v_p)_{till}$ above which the increase in the travel time through the till at large angles of incidence would be great enough to measure.

To determine an upper bound for $(v_p)_{till}$, we assume a value of $(v_p)_{till}$ and then invert the observations of $t(\hat{P}\hat{P}\hat{P}\hat{P})$ to determine the thickness of the till. By repeating this inversion for increasing values of $(v_p)_{till}$, we can determine from the goodness of fit what value of $(v_p)_{till}$ is inconsistent with our data, using an F test. F values, defined as the ratio of the sample variance of $t(\hat{P}\hat{P}\hat{P}\hat{P})$ for the model with an assumed value of $(v_p)_{till}$ to that for our standard model in which $(v_p)_{till}$ was nonunique, are shown in Table 2. Standard statistical tables show that for 90 degrees of freedom, $F > 1.3$ implies a significant difference at the 90% confidence level; for our data (Table 2), $F < 1.3$ implies $(v_p)_{till} < 1700$ m s^{-1}. The existence of $\hat{S}\hat{S}\hat{S}\hat{S}$ (to be discussed below) implies that a reasonable range for $(v_p)_{till}$ is 1550 $\pm$ 150 m/s; the till thickness is then 7.6 $\pm$ 0.8 m.

An inversion procedure similar to that described for $t(\hat{P}\hat{P})$ and $t(\hat{P}\hat{P}\hat{P}\hat{P})$ was applied to about 40 observations of $t(\hat{S}\hat{S})$ and $t(\hat{S}\hat{S}\hat{S}\hat{S})$. The model parameters were again a_{ice}, b_{ice}, a_{till}, and h_{till} as well as $(v_s)_{ice}$ and $(v_s)_{till}$; $v_s(z)$ for the firn was assumed to be as given in Table 1.

The values of the three model parameters resulting from the inversion of $t(\hat{S}\hat{S})$ were

$$a_{ice} = -0.001 \pm 0.001$$

$$b_{ice} = 1053 \pm 1\ \text{m}$$

$$(v_s)_{ice} = 1944 \pm 2\ \text{m s}^{-1}$$

with

$$s^2(\hat{S}\hat{S}) = 5.9 \times 10^{-7}\ s^2$$

which gives a standard deviation (0.8 ms) that is close to the estimated picking error for S waves.

Similarly, the inversion of $t(\hat{S}\hat{S}\hat{S}\hat{S})$ gave

$$a_{till} = 0.000 \pm 0.002$$

$$h_{till} = 8.4\ \text{m} + (0.053\ \text{s})[(v_s)_{till} - 160\ \text{m s}^{-1}] \quad (6)$$

$$s^2(\hat{S}\hat{S}\hat{S}\hat{S}) = 1.4 \times 10^{-5}$$

which implies a standard deviation (3.7 ms) that is several times the estimated picking error. Because, as mentioned above, $(v_s)_{till}$ is an order of magnitude less than $(v_p)_{till}$, an analysis like that done for $(v_p)_{till}$ to determine a maximum $(v_s)_{till}$ does not yield a useful upper bound. A better approach is simply to assume that h_{till} derived from the P wave analysis is correct and substitute it in equation (6); this gives $(v_s)_{till} = 145 \pm 15$ m s^{-1}. The larger sample variance for $t(\hat{S}\hat{S}\hat{S}\hat{S})$ may be due to an increased sensitivity to roughness at the base of the till that results from this very low S wave velocity in the till.

3.4. Discussion of Model Parameters

The slopes for the upper and lower boundaries of the till derived from the independent analyses of P and S wave reflections are not significantly different. Both boundaries are very nearly parallel to the surface; there is at most a relative downstream dip of 0.1°.

The ice thickness calculated from the S waves is approximately 20 m greater than that calculated from the P waves. The value resulting from the P wave analysis is more accurate because this

discrepancy is almost certainly due to a slight anisotropy in the ice. Observation of a small amount of shear wave splitting in both active and passive seismic experiments at UpB shows that a slight anisotropy (at most 2%) exists in the ice of ice stream B [Bentley et al., 1987; Blankenship et al., 1987]. A greater anisotropy in v_s than in v_p is to be expected because S waves are far more sensitive to a preferred crystal orientation than P waves [Bennett, 1968; Bentley, 1971].

The measured value $(v_p)_{ice} = 3831$ m s^{-1} can be used in the relationship defined by Kohnen [1974], which is based on isotropic ice, to estimate a mean temperature in the solid ice of -16 ± 2°C. That is consistent with an approximate mean temperature, -20°C, one can calculate by assuming a constant temperature of -26°C in the top half of the ice and below that a linear increase to the pressure melting point at the base. This agreement suggests that there is little P wave anisotropy in the ice stream.

In the remainder of this paper we will be considering only the velocities in the subglacial layer. We will therefore designate the maximum values for $(v_p)_{till}$ and $(v_s)_{till}$ that we have determined simply by $(v_p)_{max}$ and $(v_s)_{max}$.

4. Derivation of Properties

We next use $(v_p)_{max} = 1700$ m s^{-1} and $(v_s)_{max} = 160$ m s^{-1} in the subglacial layer to estimate some of the physical properties of the sediment. In a porous, saturated sediment v_p depends primarily on the porosity n (and therefore the density), whereas v_s is most sensitive to the effective (or intergranular or differential) pressure [Hamdi and Taylor Smith, 1982]. The effective pressure ΔP is the difference between the pore water pressure, which tends to weaken the contact between the grains, and the overburden pressure, which tends to force the grains more tightly together, thus increasing the rigidity of the solid framework of the sediment. In our case the overburden pressure is simply the glaciostatic pressure of the overlying ice, which at UpB is 9×10^6 Pa (90 bars).

Our first approach is to estimate the minimum porosity n_{min} from $(v_p)_{max}$ through matching the seismically determined bulk modulus

$$\kappa = \rho v_p^2 \qquad (7)$$

where ρ is bulk sediment density, with the bulk modulus that can be calculated from Biot theory. From Hamdi and Taylor Smith [1982, equation 3]:

$$\kappa = \frac{1 - R^2}{(1 - n - R)\, C_s + nC_w} + \frac{1}{C_f} + \frac{4}{3}\,\mu \qquad (8)$$

where C_s, C_w, and C_f are the compressibilities of the sedimentary particles, the water, and the sedimentary frame, respectively; μ is the shear modulus, given by $\mu = \rho v_s^2$; and $R = C_s/C_f$. For a typical rock particle we take $C_s = 2.6 \times 10^{-11}$ Pa^{-1}; for fresh water at -1°C under glaciostatic pressure $v_p = 1412$ m s^{-1} [Clay and Medwin, 1977, p. 88], whence $C_w = 5.0 \times 10^{-10}$ Pa^{-1}. C_f has been calculated from the empirical relation $C_f = 0.0275\, v_s^{-2.63}$ [Hamdi and Taylor Smith, 1982] using $v_s = 160$ m s^{-1} to give $C_f = 4.4 \times 10^{-8}$ m^2 Pa^{-1}. Then $R = 6 \times 10^{-4}$, and to better than 1%, (8) reduces to

$$\kappa = [(1 - n)\, C_s + nC_w]^{-1} + \frac{4}{3}\,\rho\, v_s^2 \qquad (9)$$

We do not know ρ a priori, so we let $\rho = (1-n)\rho_s + n\rho_w$, where $\rho_s = 2.6 \times 10^3$ kg m^{-3} is the density of the sediment particles and $\rho_w = 1.0 \times 10^3$ kg m^{-3} is the density of the interstitial water. Equating (7) and (9) for $(v_p)_{max} = 1700$ m s^{-1} then gives $n_{min} = 0.30$.

Next we wish to make comparisons of our $(v_p)_{max}$ with laboratory measurements; to do so, we first must correct for the wave speed in the constituent water. Most of the values of v_p in the literature refer to marine sediments saturated with seawater and are cited approximately for standard laboratory conditions. For seawater with a salinity of 35‰ at 20°C and atmospheric pressure, $v_p = 1522$ m s^{-1} [Clay and Medwin, 1977, p. 88], compared to $v_p = 1412$ m s^{-1} in fresh water at subglacial pressure. Because our measured velocity is so low, it clearly must be dominated by the sound velocity in water; so to compare our velocity with the laboratory measurements, we add a (rounded) correction of 100 m s^{-1}, giving a corrected $(v_p)_{max}$ in the layer of 1800 m s^{-1}.

Allowance also should be made for the frequency effect in measuring v_p. Most laboratory measurements are made at frequencies between 100 kHz and 1 MHz, whereas our seismic frequencies are only about 400 Hz. Standard Biot theory [Biot, 1956; Hamdi and Taylor Smith, 1982] shows that there is a rather abrupt transition from a low-frequency wave speed $(v_p)_0$ to a high-frequency wave speed $(v_p)_\infty$ around a frequency f_c that depends on the hydraulic conductivity $\emptyset$ according to the approximate relation

$$f_c \approx \frac{gn}{2\pi\emptyset}$$

where g is the acceleration of gravity. For sands and sandy silts, $\emptyset = 0(10^{-5}$ m s$^{-1})$ [Freeze and Cherry, 1979; Hamdi and Taylor Smith, 1982], so $f_c \approx 0$(100 kHz). Thus for laboratory measurements on sandy sediments at frequencies over 100 kHz, it is likely that $(v_p)_\infty$ will be measured. The difference between $(v_p)_\infty$ and $(v_p)_0$ for sandy sediments is about 100 m s^{-1} [Hamdi and Taylor Smith, 1982]. On the other hand, for sediments with an order of magnitude or more lower hydraulic conductivity (i.e., silts and muds [Freeze and Cherry, 1979]), $f_c \gtrsim 500$ kHz, and the frequency effect can be ignored for measurement frequencies of a few hundred kilohertz. Two of the experimental results discussed below refer to sands, so a velocity correction of 100 m s^{-1} has been applied; none was applied in the other cases. However, as the actual hydraulic conductivities of the samples on which the velocity measurements were made are not known, there remains a considerable uncertainty in the correction for the frequency effect. We believe that a standard error of ± 50 m s^{-1} is conservative for this correction.

We now compare our $(v_p)_{max}$ with several experimental results. The results of these com-

TABLE 3. Minimum Porosities Calculated by Comparing $(v_p)_{max}$ From Ice Stream B With Laboratory Measurements

Sample	f (kHz)	n_{min}	Error	Reference
Marine sediments	200	0.35	±0.10	Hamilton [1970]
Lake Erie sediments	330	0.33	0.05	Morgan [1969]
Clayey silt	400	0.30	0.06	Anderson [1974]
Shallow water clayey silt	400	0.33	0.05	Anderson [1974]
Sand	1000	0.32	0.04	Hamdi and Taylor Smith [1981]
Artificial sands	250	0.28	0.03	Schultheiss [1983]
Means		0.32	0.02	

Here f is the source frequency in the laboratory measurements. See text for further explanation.

parisons are described below and summarized in Table 3.

Hamilton [1970] presents a compilation of many measurements at 200 kHz on a variety of shallow water marine sediments, mostly silts and silty clays. For $(v_p)_{max}$ = 1800 m s^{-1}, we find $n_{min} = 0.35 \pm 0.10$.

Morgan [1969] made measurements in Lake Erie silts and clays with a 3-μs pulse. The sound speed in the water was 1530 m s^{-1}, which is close enough to that for our assumed standard salt water that no additional correction need be applied. His regression relation gives $n_{min} = 0.33 \pm 0.05$.

Anderson [1974] made measurements at 400 kHz on fine-grained marine sediments. Using his velocity equation 1b and $(v_p)_{max}$ = 1800 m s^{-1} yields $n_{min} = 0.31 \pm 0.06$. If instead we use his expression for shallow water sediments only (his Table 4, water depth < 1500 m), then $n_{min} = 0.33 \pm 0.05$.

Hamdi and Taylor Smith [1981] show v_p as a function of void ratio in sand at f = 1 MHz. The velocity correction of 100 m s^{-1} is applied in this case; for corrected $(v_p)_{max}$ = 1900 m s^{-1}, $n_{min} = 0.32 \pm 0.04$.

Schultheiss [1983] made measurements at 250 kHz on artificial sands, including both samples with a narrow range of grain sizes and samples with a wide range. Grain sizes were between about 0.1 and 1.0 mm. The two kinds of samples yielded indistinguishable velocity-versus-porosity curves. Here again we assume that the measured v_p was $(v_p)_\infty$; a corrected $(v_p)_{max}$ = 1900 m s^{-1} yields $n_{min} = 0.28 \pm 0.03$.

The mean regression lines of v_p versus n from the references cited are shown in Figure 5. Curve 1 [Hamilton, 1970] is substantially higher than most of the others at higher porosities but is close to them around our $(v_p)_{max}$. Curve 5 from Hamdi and Taylor Smith [1981] is also high, but the frequency effect seems to provide a satisfactory explanation because the corresponding porosity estimate is close to the others. On the other hand, the frequency correction appears of questionable validity when applied to the data from Schultheiss [1983], since his curve (curve 6) is very close to the (presumably) $(v_p)_0$ curves 2, 3, and 4. Nevertheless, the estimates of the minimum porosity are in reasonably good agreement, not only with each other but with the estimate from Biot theory cited earlier.

The error estimate for n_{min} has two parts, the error in the frequency correction, ±50 m s^{-1}, and the scatter in the experimental data relating v_p to n. To get the latter component, we take the estimates from four of the five papers with which we have made comparison: ±40 m s^{-1} [Hamilton, 1970], ±54 m s^{-1} [Morgan, 1969], ±35 m s^{-1} [Anderson, 1974], and ±51 m s^{-1} [Hamdi and Taylor Smith, 1981]. Schultheiss [1983] gives no estimate. As the four estimates are not significantly different, we adopt the average, ±45 m s^{-1}, for all our comparisons. Combining the two parts, we get ±70 m s^{-1} for the error (in terms of velocity) in the n versus v_p relationship. This error was used to get the corresponding errors in n_{min} (Table 3) and has been treated as randomly distributed in calculating the error in the mean. The mean porosity that we have calculated in Table 3 is unweighted because each estimated error reflects simply the slope of the corresponding regression curve (Figure 5), rather than any indication of the accuracy of the corresponding experiment.

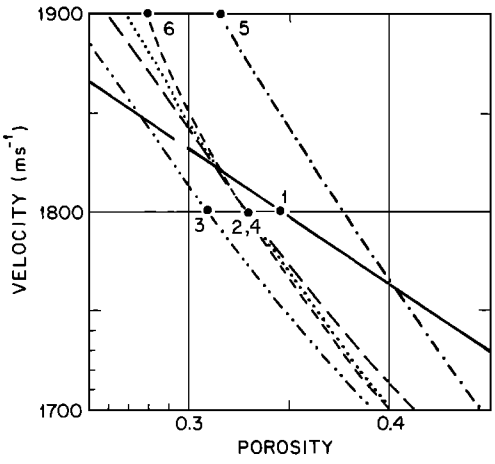

Fig. 5. Plot of relationships between v_p and n from laboratory experiments. Numbers denoting the experimental curves are placed by the solid circles that mark the v_p and n appropriate to our field determination of $(v_p)_{max}$. For further explanation, see text. Curves are from (1) Hamilton [1970], (2) Morgan [1969], (3 and 4) Anderson [1974], (5) Hamdi and Taylor Smith [1981], and (6) Schultheiss [1983].

TABLE 4. Effective Pressures Calculated by Comparing $(v_s)_{max}$ as Measured on Ice Stream B With Laboratory Measurements

Sample	$(\Delta P)_{max}$, kPa	Reference
Artificial sand	40	Schultheiss [1983]
Silt	70	Schultheiss [1981]
Silty clay	30	Schultheiss [1981]
Potter's clay	130	Schultheiss [1981]
Sands	20	Hamilton [1976]
Marine silt-clays	70 ± 50	Hamilton [1976]
Sands	30	Ohta and Goto [1978]
Clays and silts	60	Ohta and Goto [1978]
Mean	60 ± 40	

We conclude that the porosity in the layer beneath ice stream B is greater than 0.32 ± 0.02.

The other quantity that we wish to estimate is the effective pressure ΔP since ΔP is critical to the shear strength of the medium. The best measure of ΔP is v_s because in an unconsolidated sediment v_s depends principally on the intergranular friction and therefore on the intergranular pressure. Table 4 summarizes the comparison of ΔP versus v_s described below.

Experiments were carried out by Schultheiss [1983] on one of the artificial sand samples previously mentioned to determine v_s as a function of ΔP. His sample had a porosity of 0.35. At very low effective pressure (~5 kPa), v_s was close to 50 m s^{-1}; v_s = 160 m s^{-1} was attained at ΔP = 40 kPa. Other measurements by Schultheiss [1981] result in estimates of $(\Delta P)_{max}$, for $(v_s)_{max}$ = 160 m s^{-1}, of 70 kPa for silt, 30 kPa for silty clay, and 130 kPa for potter's clay.

Another approach comes from Hamilton [1976], who presents a compilation of v_s curves as a function of depth in marine sediments. To relate depth z to differential pressure, we use the relation $\Delta P = (\rho - \rho_w)gz$. For sands, Hamilton's [1976] equation 8 and Figure 1 both yield $\Delta P \approx$ 20 kPa. For silt-clays and turbidites his Figure 2 implies v_s = 160 m s^{-1} at a mean depth of around 10 m, corresponding to $\Delta P \approx$ 70 kPa. A study on the alluvial plains of Japan [Ohta and Goto, 1978] yielded similar results: depths of ~3 m (~30 kPa) for sands and ~8 m (~60 kPa) for clays and silts.

Of the references cited, only Hamilton [1976] gives an idea of the scatter in ΔP corresponding to a fixed value of v_s. His Figure 2 shows a range of experimental curves from which we estimate an uncertainty of ±50 kPa for ΔP. Lacking any other error estimates, we adopt that figure for all the determinations of $(\Delta P)_{max}$ in Table 4. The mean value of $(\Delta P)_{max}$ is then 60 ± 40 kPa.

We can also estimate $(\Delta P)_{min}$ corresponding to $(v_s)_{min}$, which we get in turn by requiring $v_p >$ 1412 m s^{-1}, the sound speed in water. Then $(v_s)_{min}$ = 130 m s^{-1}, and $(\Delta P)_{min} \approx$ 40 kPa. Thus for our best estimate of ΔP we take 50 ± 40 kPa.

Having obtained an estimate of ΔP, we can now go further in estimating n. Schultheiss' [1983] experiments showed a definite tendency for n to be greater for a given v_s as the constituent particles of the sample became more irregular and mixed in size and shape. Naturally derived sediment beneath the ice stream would be likely to have a mixture of grain sizes and shapes, particularly if it is a glacial till, as seems probable. That would then imply a relatively high porosity. Schultheiss [1983, p. 24] also found v_s = 230 m s^{-1} for a sand porosity of 0.35 under a triaxial load of 60 kPa; correcting to 50 kPa [Schultheiss, 1983, Figure 8] and extrapolating by an approximate low-pressure regression slope [Schultheiss, 1983, Figure 4] yields $n \approx 0.42$ for v_s = 160 m s^{-1}.

Another indication of high porosity comes from an equation recommended for approximate engineering computations related to angular-grained materials by Richart et al. [1970, p. 154] and cited by Hamilton [1976, equation 6] (which we have corrected to SI form):

$$v_s = \frac{18.4 - 24.6n}{1 - n} \Delta P^{\frac{1}{4}} \qquad (10)$$

For v_s = 160 m s^{-1} and ΔP = 50 kPa, then n = 0.55. Although equation (10) is not expected to give a precise value, this result is another indication that n is substantially greater than n_{min}.

Finally, we compare our ratio $(v_p)_{max}/(v_s)_{max}$ to velocity ratios measured for saturated sediments at several effective pressures by Hamdi and Taylor Smith [1982]. Applying to $(v_p)_{max}$ the frequency corrections recommended in their Figure 8, we obtain, from our velocity ratio and their Table 1: n = 0.44, ΔP = 50 kPa for fine silt; n = 0.42, ΔP = 90 kPa for sandy silt; n = 0.39, ΔP = 40 kPa for fine sands; and n = 0.53, ΔP = 80 kPa for silty clay. These values of n and ΔP are unique for a given grain size and are completely consistent with those that we estimate directly from $(v_p)_{max}$ and $(v_s)_{max}$ above.

From all these results we conclude that $n \approx$ 0.4, perhaps somewhat higher, and that $\Delta P \approx$ 50 kPa. That the porosity is substantially more than 0.32 rather than 0.3 or less is the most important point; the larger porosity suggests that the till is dilated [Alley et al., 1986, this issue (a), (b)].

5. Conclusions

At least at one location, an active Antarctic ice stream is underlain by a layer of saturated sediment which Alley et al. [1986] call a till. In an area beneath ice stream B where the top and bottom of this layer are essentially parallel to the surface and the thickness of the layer is about 8 m, the till is characterized by a P wave velocity of less than 1700 m s^{-1} and an S wave velocity of less than 160 m s^{-1} (v_p/v_s = 11). The low seismic wave speeds in the layer indicate that the material has a porosity substantially greater than 0.32, probably around 0.4, and is saturated with water at a pore pressure only about 50 kPa less than the glaciostatic pressure (9000 kPa). Blankenship et al. [1986] and Rooney et al. [this issue] show that this till is also characterized by grooves in the substrate beneath it and is essentially continuous beneath ice stream B in the vicinity of UpB. For reasons that are explained further by Alley et al. [1986, this issue (a)], we believe that these characteristics indicate that the subglacial layer is deforming and eroding the stationary surface below

and that it is deformation in the layer rather than deformation in the ice or basal sliding that is the principal component of ice stream movement.

Acknowledgments. We express our thanks to B. R. Weertman, J. E. Nyquist, R. Flanders, and the Polar Ice Coring Office of the University of Nebraska at Lincoln, as well as to the other members of the University of Wisconsin field party: S. Shabtaie, D. G. Schultz, K. C. Taylor, Jr., and J. Dallman. We are also grateful to L. A. Powell, B. D. Karsh, R. B. Abernathy, W. L. Unger, and B. R. Weertman for engineering assistance and to A. N. Mares and S. H. Smith for manuscript and figure preparation. Financial support was provided by the National Science Foundation under grants DPP81-20322 and DPP84-12404. Geophysical and Polar Research Center, University of Wisconsin-Madison, contribution 453.

References

Aki, K., and P. G. Richards, Quantitative Seismology, vol. 2, 932 pp., W. H. Freeman, Calif., 1980.

Alley, R. B., D. D. Blankenship, C. R. Bentley, and S. T. Rooney, Deformation of till beneath ice stream B, West Antarctica, Nature, 322, 57-59, 1986.

Alley, R. B., D. D. Blankenship, C. R. Bentley, and S. T. Rooney, Till beneath ice stream B, 3, Till deformation: Evidence and implications, J. Geophys. Res., this issue (a).

Alley, R. B., D. D. Blankenship, S. T. Rooney, and C. R. Bentley, Till beneath ice stream B, 4, A coupled ice-till flow model, J. Geophys. Res., this issue (b).

Anderson, R. S., Statistical correlation of physical properties and sound velocity in sediments, in Physics of Sound in Marine Sediments, edited by L. Hampton, pp. 481-518, Plenum, New York, 1974.

Bennett, H. F., An investigation into velocity anisotropy through measurements of ultrasonic wave velocities in snow and ice cores from Greenland and Antarctica, Ph.D. thesis, Univ. of Wis., Madison, 302 pp., 1968.

Bentley, C. R., Seismic anisotropy of the West Antarctic ice sheet, in Antarctic Snow and Ice Studies II, Antarct. Res. Ser., vol. 16, edited by A. P. Crary, pp. 131-177, AGU, Washington, D. C., 1971.

Bentley, C. R., Antarctic ice streams: A review, J. Geophys. Res., this issue.

Bentley, C. R., S. Shabtaie, D. D. Blankenship, D. G. Schultz, S. T. Rooney, and S. Anandakrishnan, Remote sensing of the Ross ice streams and adjacent Ross Ice Shelf, Antarctica, Ann. Glaciol., 9, in press, 1987.

Biot, M. A., Theory of propagation of elastic waves in a fluid-saturated porous solid, J. Acoust. Soc. Am., 28, 168-191, 1956.

Blankenship, D. D., C. R. Bentley, S. T. Rooney, and R. B. Alley, Seismic measurements reveal a saturated, porous layer beneath an active Antarctic ice stream, Nature, 322, 54-57, 1986.

Blankenship, D. D., S. Anandakrishnan, J. L. Kempf, and C. R. Bentley, Microearthquakes under and alongside ice stream B, detected by a new passive seismic array, Ann. Glaciol., 9, in press, 1987.

Clay, C. S., and H. Medwin, Acoustical Oceanography, 544 pp., John Wiley, New York, 1977.

Dahlquist, G., and A. Björck, Numerical Methods, translated by N. Anderson, 573 pp., Prentice-Hall, Engelwood Cliffs, N. J., 1974.

Forsythe, G. E., M. A. Malcolm, and C. B. Miller, Computer Methods for Mathematical Computations, 259 pp., Prentice-Hall, Engelwood Cliffs, N. J., 1977.

Freeze, R. A., and J. A. Cherry, Groundwater, 604 pp., Prentice-Hall, Engelwood Cliffs, N.J., 1979.

Hamdi, F. A. I., and D. Taylor Smith, Soil consolidation behavior assessed by seismic velocity measurements, Geophys. Prospect., 29, 715-729, 1981.

Hamdi, F. A. I., and D. Taylor Smith, The influence of permeability on compressional wave velocity in marine sediments, Geophys. Prospect., 30, 622-640, 1982.

Hamilton, E. L., Sound velocity and related properties of marine sediments, North Pacific, J. Geophys. Res., 75, 4423-4446, 1970.

Hamilton, E. L., Shear-wave velocity versus depth in marine sediments: A review, Geophysics, 41(5), 985-996, 1976.

Kohnen, H., The temperature dependence of seismic waves in ice, J. Glaciol., 13(67), 144-147, 1974.

Menke, W., Geophysical Data Analysis: Discrete Inverse Theory, 260 pp., Academic, Orlando, Florida, 1984.

Morgan, N. A., Physical properties of marine sediments as related to seismic velocities, Geophysics, 34(4), 529-545, 1969.

Ohta, V., and N. Goto, Empirical shear wave velocity equations in terms of characteristic soil indexes, Earthquake Eng. Struct. Dyn., 6, 167-87, 1978.

Richart, F. E., Jr., R. D. Woods, and J. R. Hall, Jr., Vibrations of Soils and Foundations, 414 pp., Prentice-Hall, Englewood Cliffs, N. J., 1970.

Rooney, S. T., D. D. Blankenship, R. B. Alley, and C. R. Bentley, Till beneath ice stream B, 2, Structure and continuity, J. Geophys. Res., this issue.

Schultheiss, P. J., Simultaneous measurement of P and S wave velocities during conventional laboratory soil testing procedures, Mar. Geotechnol., 4(4), 343-367, 1981.

Schultheiss, P. J., The influence of packing structure and effective stress on V_s, V_p, and the calculated dynamic and static moduli in sediments, in Acoustics and the Sea-Bed, edited by N. G. Pace, pp. 19-27, Bath University Press, Bath, England, 1983.

Shabtaie, S., and C. R. Bentley, Ice streams and grounding zones of West Antarctica and the Ross Ice Shelf, Ann. Glaciol., 8, 199-200, 1986.

R. B. Alley, C. R. Bentley, D. D. Blankenship, and S. T. Rooney, Geophysical and Polar Research Center, University of Wisconsin-Madison, 1215 W. Dayton Street, Madison, WI 53706.

(Received July 7, 1986;
revised December 19, 1986;
accepted January 27, 1987.)